Observational Characteristics of Radio Emission Related to Multi-polar Magnetic Configuration *

Min Wang[1], Rui-Xiang Xie[1], Chun Xu[1], Shuo-Biao Shi[1] and Yi-Hua Yan[2]

[1] National Astronomical Observatories, Yunnan Observatory, Chinese Academy of Sciences, Kunming 650011; *wm@ynao.ac.cn*
[2] National Astronomical Observatories, Chinese Academy of Sciences, Beijing 100012

Abstract We present a large complex radio burst and its associated fast time structures observed on 2001 April 10 in the frequency range of 0.65–7.6 GHz. The NoRH radio image observation shows very complex radio source structures which include preexisting, newly emerging, submerging/cancelling polarities and a bipolar, a tripolar (a 'bipolar + remote unipolar'), and a quadrupolar structure. This suggests that the radio burst is generated from a very complicated loop structure. According to the spectral and image observations, we assume that the beginning of this flare was caused by a single bipolar loop configuration with a 'Y-type' reconnection structure. A composite of radio continuum and fast time structures is contained in this flare. The various fast radio emission phenomena include normal and reverse drifting type III bursts, and slowly drifting and no-drift structures. The tripolar configurations may form a double-loop with a 'three-legged' structure, which is an important source of the various types of fast time structures. The two-loop reconnection model can lead simultaneously to electron acceleration and corona heating. We have also analyzed the behaviors of coronal magnetic polarities and the emission processes of different types radio emission qualitatively. Interactions of a bipolar or multi-polar loop are consistent with our observational results. Our observations favor the magnetic reconnection configurations of the 'inverted Y-type' (bipolar) and the 'three-legged' structures (tripolar or quadrupolar).

Key words: Sun: radio radiation – Sun: activity – Sun: flares

1 INTRODUCTION

The magnetic configuration of solar flares is the key when examining the energy storage, energy release, and the particle acceleration in flares. The double-loop configuration is particularly

important because it is one of the most frequent configurations in active regions. Interactions between a newly emerging flux and an overlying magnetic field is one of the best-known conditions to cause solar flares (e.g., Hanaoka 1997). It has been found that bipolar interaction is an essential ingredient causing flares (Mandrini et al. 1991; Démoulin et al. 1993 ; Machado et al. 1998). It is indicated that interactions between coronal loops can cause both flares and microflares (Aschwanden et al. 1996b). Virtually all solar flare models involve magnetic reconnection in one form or other. Magnetic reconnection changes the topology of the magnetic field by reconfiguring the connectivity between opposite magnetic polarities.

Flare models with putative energy release sites near (or above) the loop top and energy-loss sites near the footpoints were provided and considered in some theoretical and observational models (Masuda et al. 1994; Mandrini et al. 1991; Hanaoka 1997; Nishio et al. 1997; Aschwanden et al. 1999). However, the observational verification has not been pursued completely until recently. It has also been suggested that particle acceleration occurs at sites where the ambient electron density corresponds to the plasma frequency in the decimetric range (Bastian et al. 1998). The cause of particle acceleration may be changes of magnetic field topology during the impulsive phase (Trottet 1986) and/or loop-loop interactions (Hanaoka 1997). It is well known that different flares have different energy output, different energy distributions over different frequency bands, and different evolution time scales. Thus a unified theoretical interpretation of solar flares is impossible. The different categories of flares have to be explained as resulting from basically different magnetic configurations and physical mechanisms.

In this paper we analyse the large complex radio burst that occurred on 2001 April 10, which comprised normal and reverse type III bursts, slowly drifting structures as well as stationary structures. We use data obtained with the radio spectrometers at National Astronomical Observatories of China (NAOC) in Beijing and Yunnan, the Nobeyama Radio Heliograph (NoRH; Nakajima et al. 1994), and the Michelson Doppler Imager (MDI).

The data of NoRH and MDI were downloaded from their web sites. The event was observed essentially simultaneously at microwave–decameter wavelengths, accompanied by H_α, EUV, SXR, HXR, and CMEs (see Internet Web Site: *http://sgd.ngdc.noaa.gov*). These observations are also characterized by a variability of the spatial and temporal structures at 17 GHz. Particularly, the images of polarization and intensity of radio emission allow us to make a better and more comprehensive analysis of the magnetic configuration during this radio burst.

The characteristics during the whole radio burst are described in Section 2. The evolution of radio source reflecting the related coronal magnetic structures and magnetic configurations are described in Section 3. Radio bursts and coronal magnetic configurations as well as the radio emission process and magnetic topology are analyzed in Section 4. A summary and a discussion are given in Sections 5 and 6, respectively.

2 OBSERVATIONS

2.1 Instruments

A decimetric radio spectrometer for the range 1.0–2.0 GHz and a microwave spectrometer over 2.6–3.8 GHz and 5.2–7.6 GHz at National Astronomical Observatories, Chinese Academy of Sciences (NAOC) (i.e., the former Beijing Astronomical Observatory) came into operation in 1993, 1996, and 1999, respectively (Ji et al. 1997; Ji et al. 2000). In addition, a spectrometer (0.65–1.5 GHz) at Yunnan Observatory was put into operation in July 2000. It uses a 10-m diameter antenna, with a spectral resolution of about 1.4 MHz and a time resolution of 8 ms. The dynamic range is better than 10 db. The flux and circular polarization are recorded digitally. The accuracy in the degree of polarization is better than 10%.
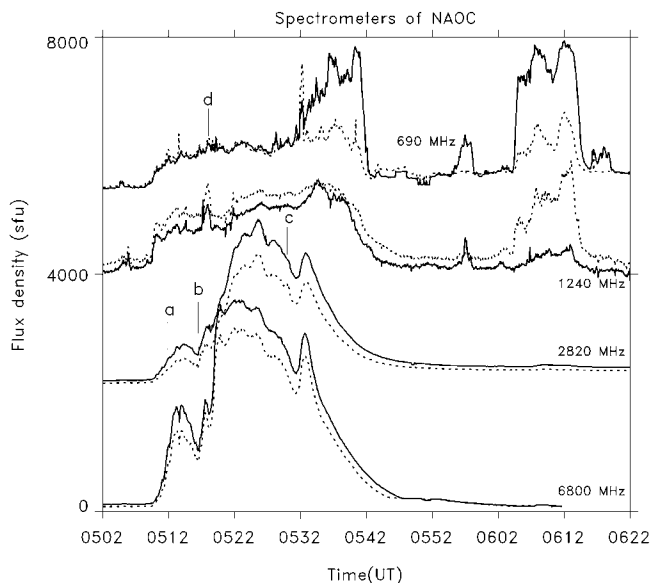
Fig. 1 Spectrogram (time profiles) of radio bursts on 2001 April 10 at selected frequencies, dashed lines for right polarization, solid lines, left polarization. Letters a, b, and c mark the times of occurrence of the fast fine structures shown in Figure 2, and d marks the fine structures displayed in Figure 3.

2.2   Characteristics of Radio Observations

The radio burst on 2001 April 10 was observed simultaneously with these four spectrometers. This radio burst was associated with a large flare (Importance 3B/X2.3, location S23 W9 in AR 9415, start about 0510 UT, maximum about 0526 UT (microwave band) and 0612 UT (decimeter band), end about 0620 UT).

Figure 1 shows the time profiles at the selected frequencies of the four spectrometers. The profiles clearly reveal two separate groups of peaks. Moreover, there are various fine time structures superimposed on a continuous emission, i.e., normal and reverse drifting type III bursts, without drifting and slowly drifting structures (Figs. 2 and 3). All of these occurred in the impulsive phase of the radio burst. However, the first groups of reverse drifting type III bursts (e.g., Fig. 2a) occurred in the earlier impulsive phase, and then several groups of normal drifting type III bursts (e.g., Fig. 2b) occurred. Also some slowly drifting (e.g., Fig. 2c) and no-drift (e.g., Fig. 3) structures occurred in this phase. We should indicate that the coronal magnetic structures were strongly varying during the impulsive phase of the radio burst. This hints at a dependence of the radio emission on the magnetic configuration (Aschwanden 2002).

3   EVOLUTION OF CORONAL MAGNETIC STRUCTURES AND   MAGNETIC CONFIGURATIONS RELATED TO RADIO BURSTS

This event comprises the appearance of very complex magnetic structures during the development of a flare. There are the preexisting radio source, some newly emerging flux, as well as the cancelling or submerging magnetic fluxes. The NoRH images of 17 GHz I and V corresponding
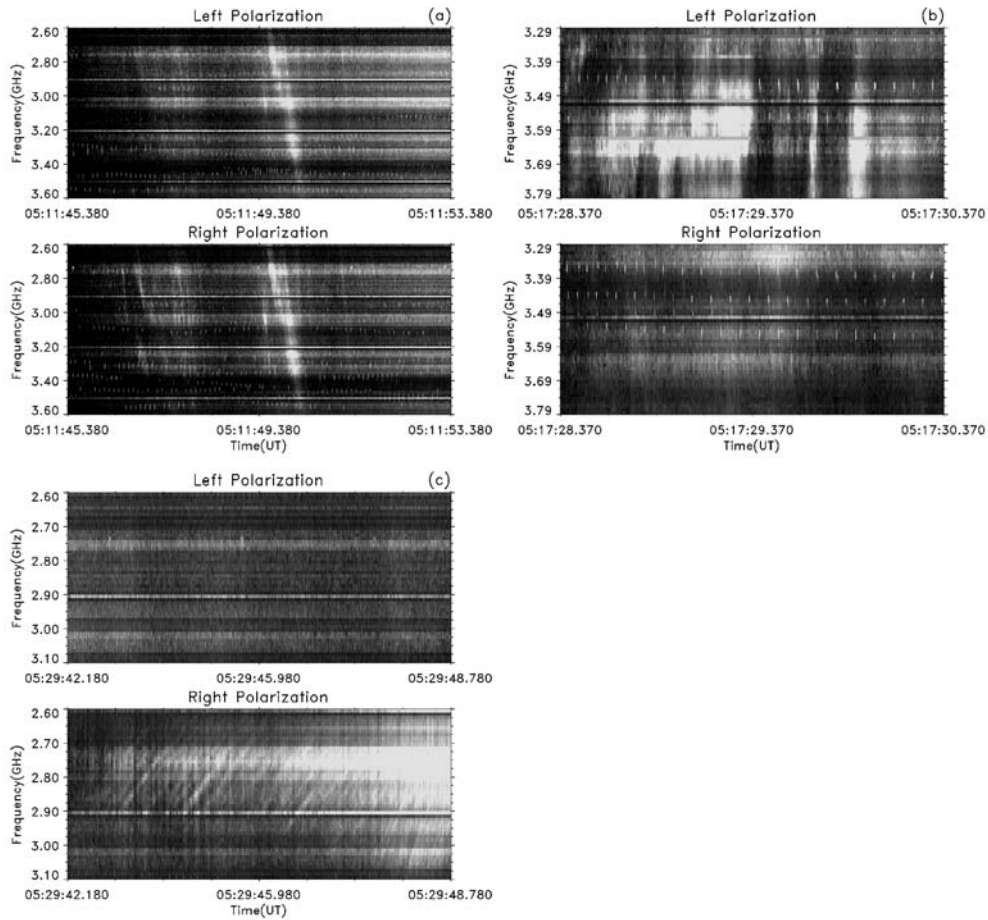
Fig. 2 Spectra of radio fast fine structures in the lower frequencies range of 2.6–3.8 GHz. (a) and (b) are type III bursts with positive and negative drift rates, (c) is a slowly drifting structure).

to the this radio burst are shown in Figures 4 and 5 as time sequences. From these images we can see the evolution of the coronal magnetic polarities at 17 GHz during the radio burst.

Figure 4a shows the preexisting magnetic unipolar (negative V) and a gradual radio source (marked by 'A') before the beginning of radio burst. This reflects the build-up process of the flare preheating (Kundu 1983); Figure 4b shows a newly emerging magnetic polarity (positive V, marked by 'B') and a radio source (marked by 'C') between the two magnetic polarities at the beginning of radio burst. Two opposite polarities may be reconnected to form an inverted 'Y-type' structure leading to the two-ribbon flare related to the broadband radio burst; Figure 4c shows a newly emerging magnetic polarity (negative V, marked by 'D') between the two original polarities.

Basing on Figure 4c, Figure 4d shows another newly emerging polarity (positive V, marked by 'E') between the two original opposite polarities. In this time there existed quadrupolar structures;
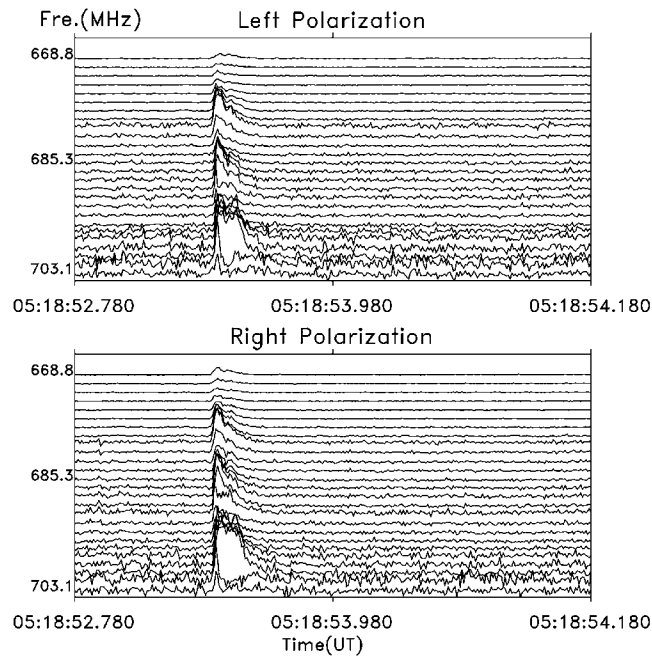
Fig. 3 Type III burst with an almost infinite drifting rate.
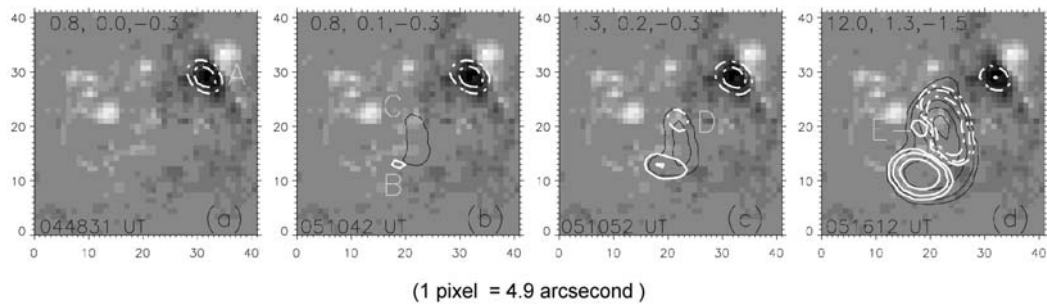

(1 pixel = 4.9 arcsecond)

Fig. 4 Evolution of NoRH radio sources at 17 GHz superposed on the MDI longitudinal component of photospheric magnetic fields. White contours and black contours represent the Stokes V and I, respectively. White solid and dotted contours represent positive and negative V, respectively. Grey scales have black-to-white ranges of –2000 and 2000 Gauss in the MDI image. The numbers in each image mark the maximum values of I, +V, and –V, in units of MK.

Figure 5a shows a disappearing polarity (original positive polar 'B'); Figure 5b shows only a positive and a negative polarity (in this time, the two original polar 'A' and 'B' had cancelled or submerged); Figure 5c shows that the submerged source 'A' re-emerged; Figure 5d shows again two polarities ('E' and 'A') with decreased strengths. We may presume that the magnetic structure as shown in Figure 5d probably caused the decimetric radio burst after several minutes, which should occur near the apex of the post flare loop.
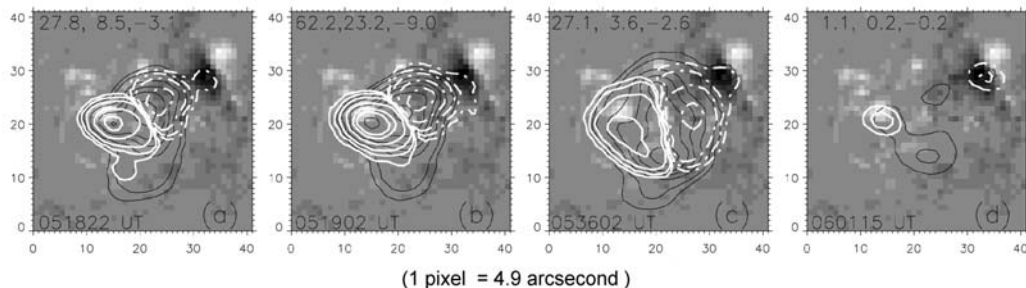
Fig. 5 Also the evolution of NoRH radio sources. The definitions of the contours and grey scales are as same as Figure 4.

4 ANALYSIS

4.1 Radio Bursts and Coronal Magnetic Configurations

We have obtained a broad band radio burst with two separate groups of peaks in the microwave and decimeter wavelengths (see Figure 1). This event is related to a global structure model of energy conversion processes, because the broad band radio burst is well correlated with the HXR, EUV, H_α and CMEs activities etc. Thus the geometries of the coronal magnetic fields could be inferred from the observations of the varying features of this complex radio source. According to the magnetic polar images (see Figs. 4 and 5), we can presume that there are single loop (bipolar in Figs. 4b and 5d) and double-loop (tripolar or quadrupolar in Figs. 4c, 4d, 5a, and 5c) magnetic configurations with a probable 'three-legged' structure, and a later multi-loop (quadrupolar in Fig. 4d) magnetic reconnection during the flare evolution (Aschwanden et al. 1999; Nishio et al. 1997; Hanaoka 1997; Aschwanden 2002). It is early seen that a considerable variety of radio emission types will be involved with a complex topology of acceleration regions and magnetic configurations. However, preexisting and newly emerging magnetic polar regions are essential for producing radio flares and microflares (i.e., radio fast time structures) (Martens & Kuin 1989).

A single bipolar loop is the outcome of an oppositely-directed bipolar reconnection process. In our analyzed case, from the evolutions (see Figs. 4 and 5) of magnetic polar images we may assume that this active region has created the double-loop or multi-loop (tripolar or quadrupolar) configurations. Also, we make use of the EUV image superposed on the polar regions of radio emission (see Fig. 6). It is clear that there are some post-flare, nested EUV loops appeared after the main phase of this flare. This is the evidence of post-flare loops. In particular, two regions with opposite polarities appeared at the beginning and end of the flare (see Figs. 4b and 5d). This means that a single bipolar loop may appear twice during the production of a double-ribbon flare. Because the radio burst (Fig. 1) seems to indicate two different energy release sites, one near the footpoints of the loop (as indicated by the microwave - decimetric burst in Fig. 1) and one near the top of the post-flare loop (the later decimetric burst in Fig. 1), a different magnetic configuration must apply to the later decimetric burst. For the microwave broadband and decimeter narrowband bursts (see Fig. 1), we can consider a certain type of bipolar flare model (e.g., caused by the structures in Figs. 4b and 5d), i.e., one with an inverted 'Y-type' structure (Aschwanden 2002; Masuda et al. 1994).
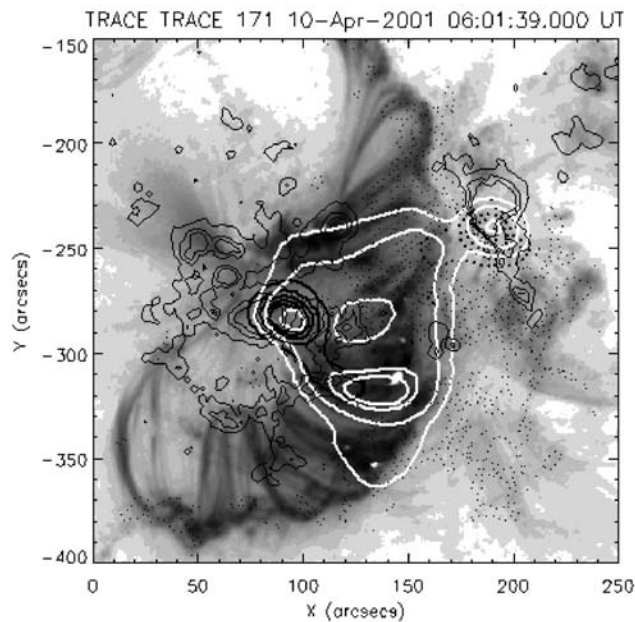
Fig. 6 TRACE image and NoRH contours associated with MDI magnetogram. The white thick solid lines are contours of brightness temperature (I) of NoRH radio sources (levels are 0.2, 0.4, 0.6, 0.8 and 1.0 MK). Black thick dotted lines are contours of brightness temperature (V) of NoRH radio sources (levels are –0.30, –0.24, –0.18, –0.12, –0.06, 0.06, 0.12, 0.18, 0.24 and 0.30 MK). The background is MDI magnetogram (thin dotted and solid lines present the negative and positive, respectively; the levels of the MDI contour are –700, –400, –100, 100, 400 and 700 Gauss).

According to the existence of the broad band (two-part, microwave and decimeter) radio burst and the EUV, X-ray, and H$_\alpha$ emissions, we can propose a comprehensive model which contains not only the 'Y-type' (bipolar) but also the tripolar (possible 'three-legged') or quadrupolar structures. In these 'Y-type' and multi-polar configurations occur both long lifetime bursts (two-ribbon flares) and various other active phenomena, such as normal and reverse drifting type III bursts, slowly and no-drift structures. However, we can suggest that the later tripolar (see Fig. 4c) may form a 'three-legged' structure of two loops, and the two loops are not anti-parallel as assumed in the traditional reconnection model. This structure could produce the later fast time structures during the impulsive phase (Hanaoka 1997).

These observational properties may be similar to those of quadrupolar magnetic reconnection in solar flares and double loop configuration of a flaring region (Aschwanden et al. 1999; Kundu et al. 2001). In this flare, two radio sources may be involved in the evolving magnetic structures. As the flare develops, the extended flaring source consisted of two regions separated in microwave and decimeter wavelengths, where first occurred the broadband microwave burst and then the narrowband decimetric one (see Fig. 1). We suggest that this decimetric burst was also caused by a single bipolar loop (the rising post-flare loop), which may occur through the development of a sheared coronal loop (c.f. Fig. 5d) (Hanaoka 1994).

Tearing mode of the sheared loop may finally occur at the intersection near the top of post-flare loop, and triggered a reconnection process responsible for the decimetric burst energy release.

4.2 Radio Emission Process and Magnetic Topology

It is generally known that the fast structures indicate (nonthermal) acceleration of energetic electrons from small magnetic structures, while the gradual continuum component represents energy release from larger magnetic structures in the form of heating (Gopalswamy et al. 1997; Parker 1988). It has also been agreed that particle acceleration sites in solar flares are generally associated with magnetic reconnection regions, or with reconnection-driven shocks. Evidence for magnetic reconnection processes in solar flares has been forthcoming over the last decade (Aschwanden 2002). Now that we have observed continuum with fast time structures, it can be inferred that there are both large and small magnetic structures during the evolution in the topology of magnetic configurations.

4.2.1 The radio continuum emission and other associated events

In our case, there were two opposite polarities at the beginning of the flare (see Fig. 4b). Therefore, we can consider the bipolar flare model where a single bipolar loop is the outcome of an oppositely-directed reconnection process (Pneuimant 1981). In this model a helmet-streamer configuration is assumed to exist at the beginning of the flare. When the field lines form an inverted 'Y-type' structure and relax, the field lines begin to reconnect. Tearing-mode instability near the 'Y-type' reconnection point triggers the flare, accelerates the particles mainly in the downward direction as well as produces shock waves (Aschwanden 2002). The accelerated particles, as soon as they leave the current sheet near the reconnection point, are injected into the flare loop and precipitate into the chromosphere along the closed field lines. The precipitating particles are responsible for the generation of HXR at the impact site, as well as H_α emission - the two ribbons. They can further cause chromospheric evaporation, which leads to the observed coronal EUV and SXR emissions (Martens & Kuin 1989). For high-energy flares Gamma-ray can also be produced (Sakai & De Jager 1991). When the accelerated electrons are trapped by the closed loop, they can emit gyrosynchrotron emission leading to broadband microwave radio burst (e.g., the beginning part of the radio burst in Fig. 1).

As regards the later decimetric burst, it may also be caused by the bipolar loop (inverted 'Y-type' structure) (see Fig. 5d). Using the observational time profile of the radio burst (Fig. 1), we can estimate the degree of polarization, to be about 70%–80% in the low frequencies (e.g., 0.69–1.24 GHz). Thus, we think that this burst in low frequencies could be attributed to the fundamental plasma emission (Aschwanden et al. 1996a; Gopalswamy et al. 1994). In fact, this post-maximum broadband burst is a mixture of gyrosynchrotron and plasma emissions, with the latter dominant because of the narrow bandwidth and the high polarization.

4.2.2 The fast time structures

Various flare observations have suggested qualitatively that solar flares result from the interaction of large scale structures (Mandrini et al. 1991). In most cases, extended flares involve several magnetic structures across the whole complex active region. The basic structure of a flare usually consists of a preexisting closed bipolar and one or more adjacent closed bipolar. It has been suggested that interaction of magnetic loops is an essential ingredient in the energy release, and the site of the interaction is the region of electron acceleration (Machado et al. 1983).

It is now clear that the acceleration region not only consist of large scale components but also many small scale elements, and that it operates intermittently in time. A spatio-temporal correlation between the time scale and flare loop size indicates a scale-invariant geometry of magnetic reconnection regions. Large shear has been observed at the onset of double-ribbon flares. This suggests that in a shear-driven burst reconnection regime, tearing mode instability and coalescence of magnetic islands can produce the intermittent episodes of acceleration (Aschwanden 2002).

Magnetic energy is stored in the reconnection regions, and is triggered under some favorable circumstances. Explosive release of the pent-up energy will lead to a variety of emissions with fast time structures (Wild et al. 1963). The primary energy release often appears as microflares or elementary flares, i.e., in the form of radio fast time structures (Benz 1985; Aschwanden et al. 1990). So radio fast time structures are often observed in a radio burst. When the fast electrons spiral downward along the field lines they can also give rise to decimetric fine structures (e.g., the reverse drifting type III burst in Fig. 2a) (Martens & Kuin 1989). A part of the accelerated electrons gets access to the open field lines and produces normal drifting type III bursts (e.g., our case in Fig. 2b).

As for the non-drifting type III burst (Fig. 3), we presume that the plasma emission may fall into the opacity frequency region for plasma emission, owing to the density enhancement due to the chromospheric evaporation front. In this frequency range the opacity changes for plasma emission are most dramatic, and the reverse-slope type III burst becomes almost infinite drifting rate (Aschwanden & Benz 1995, 1997).

As for the drifting type III bursts, the plasma radiation and the electron cyclotron maser (ECM) are the most favored mechanisms for the normal radio type III bursts and reverse drift type III bursts, respectively (Stähli & Benz 1987). In the former we expect upwards propagating electron beams in quadrupolar reconnection configuration; in the latter we expect downwards propagating electron beams in bipolar and tripolar magnetic reconnection configurations (Aschwanden 2002). Alternatively, type III bursts are caused by instabilities resulting from coupling between material flow and magnetic field topology. As a consequence of such an instability a turbulent energy cascade to small characteristic lengths grows, which produces electron acceleration at different levels leading to the type III bursts (Carbone et al. 1987).

With respect to the slowly drifting structure (Fig. 2c), it may be connected with plasmoid ejection, and may be generated by the superthermal electrons accelerated in the burst regime of the magnetic field reconnection. Alternatively, it can be explained by a plasmoid propagation upwards in the solar corona towards lower plasma densities (Karlický, Fárník & Mészárosová 2002).

5 SUMMARY

The main properties of this radio burst are: it consists of a complex radio continuum, normal and reverse drifting type III bursts, and slow and non-drifting structures. Single polar, bipolar, tripolar, and quadrupolar magnetic structures were found during the burst. Our analysis confirms that the single-loop (bipolar) configuration produced by the newly emerging flux causes a double-ribbon flare, and a later decimetric narrow band burst. Various radio fast time structures could be related to a multi-polar (tripolar or quadrupolar) structure.

These radio fast time structures reflect the fact that particles are heated and/or accelerated in compact magnetic flux loops that arise from regions of bipolar or tripolar magnetic structures. Observational results have confirmed the correlation of radio emission with coronal magnetic configuration: complex radio bursts correspond to complex coronal magnetic structures. Our observations support the models of 'Y-type' with bipolar and 'three-legged' with tripolar or
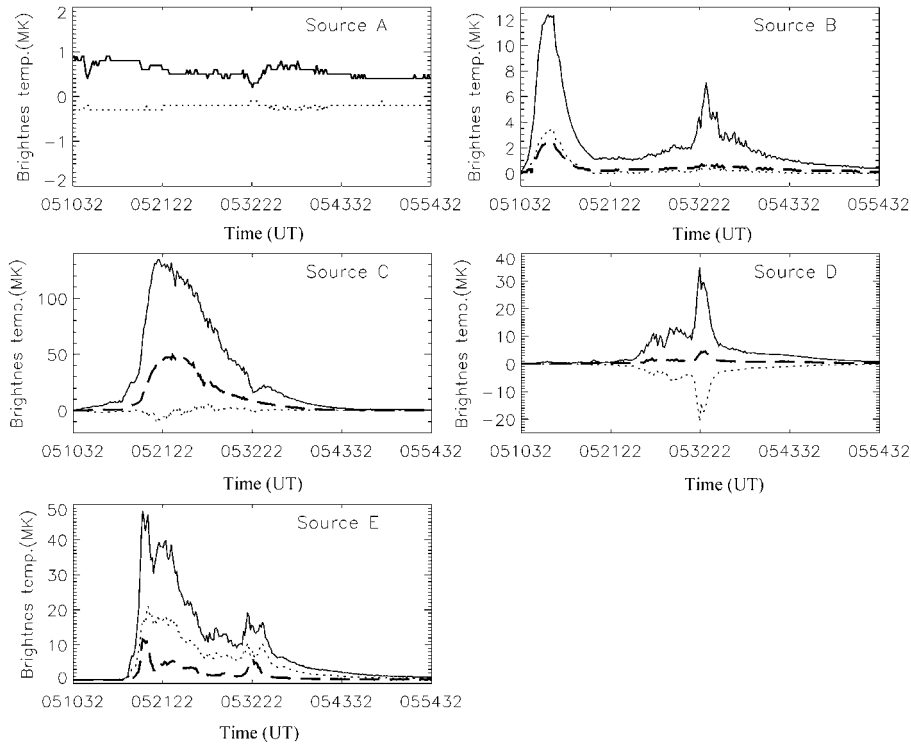
Fig. 7 Time profiles of the different radio source indicated in Figure 5. Thin solid and thin dotted lines display I and V at 17 GHz, the thick dashed lines, I at 34 GHz.

quadrupolar structures. The former can cause radio bursts of long duration, the later, short/fast radio burst.

6   DISCUSSION

(1) The relationship of complex radio burst with coronal magnetic topology. The time profile of the radio burst indicates a complex morphology. This is attributed to the result of super-imposition of emissions of several radio sources in this extended active region (see Fig. 7). In fact, these different sources are manifestations of the magnetic configuration topology and its evolution. The emission of these sources appears at different times. This means that multiple polarity magnetic structures have different interactions or reconfigurations, and the coronal magnetic configuration continues to evolve while the flare develops. Thus, the complex radio burst corresponds to a complex magnetic configuration.

(2) The lack of fast time structures at the decay phase of the microwave radio burst. The reason for a lack of fast time structures involves both the properties of flare (Priest 1981; Pneumant 1981) and the types of current loop coalescence (Sakai & De Jager 1991). When the current sheet forms during the reconnection of two opposite magnetic fields, the resulting anomalous resistivity causes the current sheet to expand rapidly. An induced electric field is therefore generated, which forces the electrons in the current sheet to behave in a runaway man-ner and/or to generate high-frequency turbulence. The fast particles are thus accelerated either

directly or stochastically (Priest 1981). In addition, the field has relaxed, and the photospheric motions of the magnetic footpoints go again to build up the force-free field after production of the two-ribbon flare (Priest 1981).

References

Aschwanden M. J., Benz A. O., Schwartz R. A., Lin R. P., Pelling R. M., Stehling W., 1990, Solar Physics, 130, 39
Aschwanden M. J., Benz A. O., 1995, ApJ, 438, 997
Aschwanden M. J., Hudson H., Kosugi T., Schwartz R. A., 1996a, ApJ, 464, 985
Aschwanden M. J., Wills M. J., Hudson H. S., Kosugi T., Schwartz R. A., 1996b, ApJ, 468, 398
Aschwanden M. J., Benz A. O., 1997, ApJ, 480, 825
Aschwanden M. J., Kosugi T., Hanaoka Y., Nishio M., Melrose D. B., 1999, ApJ, 526, 1026
Aschwanden M. J., 2002, Space Science Reviews, 101/1-2, 1
Aschwanden M. J., Pontieu B. D., Schrijver C. J., Title A. M., 2002, Solar Phys., 206, 99
Benz A. O., 1985, Solar Phys., 96, 357
Carbone V., Einaudi G., Veltri P., 1987, Solar Phy., 111, 31
Démoulin. P., van Driel-Gesztelyi L., Schmieder B., Hénoux J. C., Csepura G., Hagyard M. J., 1993, A&A, 271, 292
Gopalswamy N., Kundu M. R., Raoult A., Pick M., 1994, Solar Phys., 150, 317
Gopalswamy N., Zhang J., Kundu M. R., Schmahl E. J., Lemen J. R., 1997, ApJ, 401, L115
Hanaoka Y., 1994, ApJ, 420, L37
Hanaoka Y., 1997, Solar Phys., 173, 319
Ji H. R., Fu Q. J., Lao D. B., 1997, Acta Astrophys. Sinica, 17, 219
Ji H. R., Fu Q. J., Liu Y. Y., 2000, Acta Astrophys. Sinica, 20, 209
Karlický M., Fárník F., Mészárosová H., 2002, A&A, 395, 677
Kundu M. R., 1983, Solar Phys., 86, 205
Kundu M. R., Grechnev V. V., Garaimov V. I., White S. M., 2001, ApJ, 563, 389
Machado M. E., Somov B. V., Rovira M. G., De Jager C., 1983, Solar Phys., 85, 157
Machado M. E., Moore R. L., Hernandez A. M., Rovira M. G., Hagyard M. J., Smith J. B., 1998, ApJ, 326, 425
Mandrini C. H., Démoulin P., Hénoux J. C., Machado M. E., 1991, A&A, 250, 541
Martens P. C. H., Kuin N. P. M., 1989, Solar Phys., 122, 263
Masuda S., Kosugi T., Hara H., Tsuneta S., Ogawara Y., 1994, Nature, 371, 495
Masuda S., Tsuneta S., 1995, Publ. Astron. Soc. Japan, 47, 677
Nakajima H. et al., 1994, Proc. IEEE, 82, 705
Nishio M., Yaji K., Kosugi T. et al., 1997, ApJ, 489, 976
Parker E. N., 1988, ApJ, 330, 474
Pneumant G. W., 1981, In: E. R. Priest, ed., Solar Flare Magnetohydrodynamics, New York: Gordon and Breach, p.379
Priest E. R., 1981, In: E. R. Priest, ed., Solar Flare Magnetohydrodynamics, New York: Gordon and Breach, p.139
Sakai J-I., Ohsawa Y., 1987, Space Sci. Rev., 46, 113
Sakai J-I., De Jager C., 1991, Solar Phys., 134, 329
Stähli M., Benz A. O., 1987, A&A, 175, 271
Wentzel D. G., 1982, ApJ, 256, 271
Wild J. P., Smerd S. F., Weiss A. A., 1963, Ann. Rev. Astron. Astrophys., 1, 291